



Operation parameters multi-objective optimization method of large vertical mill based on CFD-DPM



Rongjie Huang^a, Yaoshuai Ma^a, Hao Li^{a,*}, Chunya Sun^{a,*}, Jun Liu^b, Shuai Zhang^c, Haoqi Wang^a, Bing Hao^b

^a Henan Key Laboratory of Intelligent Manufacturing of Mechanical Equipment, Zhengzhou University of Light Industry, Zhengzhou, Henan 450002, China

^b CITIC Heavy Industries Co., Ltd, Luoyang, Henan 471003, China

^c University of Greenwich, Park Row, London SE10 9LS, United Kingdom

ARTICLE INFO

Article history:

Received 27 August 2022

Received in revised form 19 January 2023

Accepted 15 March 2023

Keywords:

Particle-fluid system

Numerical simulation

Kriging

CFD-DPM coupling method

Rosin-Rammler distribution

ABSTRACT

The association mechanism between the main operation parameters and multi-physical fields of the large-scale vertical mill system is unclear, which leads to the difficulty in optimizing operation parameters to improve the performance of large vertical mill systems. To investigate the mechanism of multi-physical field coupling in the operation of the large vertical mill, the numerical simulation method is constructed by coupled CFD-DPM model to calculate the finished product quality, the simulation results were in good agreement with the actual operation results. Based on the Kriging surrogate model, a multi-objective optimization framework for large vertical mills is proposed. Finally, the multi-objective optimization design of LGM large vertical mills is carried out. Combined with CFD-DPM coupling method is developed, design variables and output responses are determined. The Kriging method is used for correlation analysis. The multi-objective optimization function was established. The NSGA-II optimization algorithm was used to update the surrogate model and obtain the optimal solution, and the optimized operating parameters increased the vertical mill yield by 5.34% and the specific surface area by 9.07%. The maximum relative error between the simulated value and the optimized value is 2.02% through numerical calculation, which verifies the superiority of the optimization method of large vertical mill for performance improvement.

© 2023 Society of Powder Technology Japan Published by Elsevier B.V. This is an open access article under the CC BY-NC-ND license (<http://creativecommons.org/licenses/by-nc-nd/4.0/>).

1. Introduction

A large vertical mill is a piece of major equipment in cement, mining, building materials, metallurgy, chemical industry, and other industries. Large vertical mills integrate the functions of drying, crushing, grinding powder selection, and transportation. The technological process is a typical coupling process integrating fluid, particles, temperature, and other multi-physical fields [1,2]. When the vertical mill is running, a large-scale particle–fluid coupling system is formed inside it. The complex structure of the cavity space inside a large vertical mill leads to a strongly coupled fluid–particle multiphase flow as a whole. There are also the sudden expansion jets at the nozzle ring, cylindrical winding flow at a certain angle of attack, shrinking flow in the gravity classification zone, and forced vortex flow in the centrifugal separation zone. The above reasons lead to an unclear correlation mechanism between the fluid field patterns of gas and solid mixtures. The existing cal-

culational models and methods are difficult to describe the coupling relationships between these parameters [3].

The large-scale vertical mill system has complex turbulent motion in its operation. To address this challenge, we must consider factors in multidiscipline, including computational fluid dynamics, multiphase flow theory, aerodynamics, etc. Algebraic stress models, $k-\epsilon$ models, RNG $k-\epsilon$ models and Reynolds stress models are usually used [4]. Scholars have studied the flow field characteristics of vertical mills. Bhasker [5] described the meshing process of vertical mill fluid simulation and used the gas–solid two-phase flow method to simulate the vertical mill and obtain the complete trajectory of the gas–solid two-phase flow from the inlet to the outlet of the vertical mill. Kozołub et al. [6] used the hybrid Euler-Lagrange method to establish a numerical calculation model of the gas–solid two-phase bi-directional coupling. They simulated the flow state in a cyclone separator under high-speed particle load. Vuthaluru et al. [7] used the Eulerian-Eulerian method to affect multiphase flow in a simplified model. Dou et al. [8] used CFD to simulate the flow field of a vertical mill and analyzed the causes of considerable differential pressure in the vertical mill.

* Corresponding authors.

E-mail addresses: lihao@zzuli.edu.cn (H. Li), 2019056@zzuli.edu.cn (C. Sun).

The study of the flow field cannot carry out multidimensional coupling analysis of the system, so scholars began to study the coupled particle–fluid system. Toneva et al. [9] used particle image velocimetry to study the particle motion in the size range of 29~573 μm in a gas–solid two-phase flow in a mill cavity separator and found that the particle motion in the grinding zone was not affected by the circumferential velocity of the separator. Mori et al. [10] used symbolic distance functions and immersed boundary methods to simulate arbitrarily shaped wall boundaries in gas–solid two-phase flows and demonstrated the applicability of the coarse-grained discrete element method in complex-shaped domains by comparing experimental and numerical analysis results. Zamani et al. [11] used a two-way coupled Euler–Lagrange method to study the corrosion phenomenon of bends due to gas–solid two-phase turbulent flow and found that the particle rotation strongly influence the corrosion rate. The particle rotation had a significant influence on the particle movement path. Carlos et al. [12] investigated a computational fluid dynamics discrete element method for interacting between gas–particle flow and non-homogeneous catalytic chemical reactions encountered in large complex particle–fluid equipment. It was found that the slip velocity and axial gas dispersion of the system were directly related to the formation of particle clusters. Elsayed et al. [13] simulated the effect of four different dust discharge structures on the internal flow field of complex particle–fluid equipment and found that there were errors of 10% and 35% in the Euler number and cut particle size, respectively. Liu et al. [14] used the two-way coupling method. The discrete phase DPM model was used to study and analyze the classification and screening characteristics of particles from three aspects: velocity field, pressure field and discrete phase distribution.

In summary, there are a series of challenges and difficulties in optimizing and controlling the operating parameters of large vertical grinding systems, which have a complex internal structure and involve the coupling of multiple physical fields such as gas, solid particles, and heat transfer. Euler's method can be used to simulate the coupling of continuous medium and fluid for the vertical mill's internal particles and simulate the particle phase's flow state. Still, it can't get the trajectory of particles. DPM method can obtain the trajectory of particles, but it consumes substantial computational resources, so it is difficult to simulate a large-scale particle–fluid system. The CFD–DPM coupling model simulates the internal flow field of the system. DPM model simulates the movement of particles in the flow field, and the particles in the flow field are modeled and tracked as packages to reduce the demand for computing resources and improve computing efficiency.

In this paper, a large vertical mill was taken as the research object. We investigate the effects of operating parameters on the powder particle classification and particle size distribution, and the fineness of finished products under the particle–fluid coupling effect. And the optimization method of the operating parameters. Based on Computational Fluid Dynamics (CFD), the Discrete Phase Model (DPM) is used to calculate the trajectory of particles in the flow field numerically. A multi-objective optimization model for large vertical mill operating parameters is established based on the Kriging surrogate model method. Finally, the operation parameters of an LGM large vertical mill are optimized. The optimization results show that the method is effective.

The contents of this paper are organized as follows: Section 1 briefly introduces the structure of large vertical mill and designs a multi-objective optimization framework for a large vertical mill based on CFD–DPM. Section 2 describes the numerical model of the granular fluid system based on CFD–DPM. Section 3 introduces the DOE experimental design. In Section 4, the Kriging method is introduced and cross-verified, which proves the feasibility of Kriging method. Section 5 designs the optimized process. In Section 6,

an example is verified and the results are analyzed. Chapter seven summarizes the work done.

2. A multi-objective optimization framework of large vertical mill based on CFD–DPM

2.1. Working principle of large vertical mill

A large vertical mill comprises tens of thousands of parts, and its complex particle–fluid system parameters include mechanical, electrical, hydraulic, and other disciplines. It has a complex model structure, many monitoring operation points, and a long product life cycle, making it challenge to develop and design the system, process and assemble the parts and maintain the equipment. This paper uses a large vertical mill as the research object for numerical simulation. Its grinding roller is a flat cone roller loaded with curved arms. The grinding roller device adopts the arrangement of four grinding rollers, and the main roller and the auxiliary roller are symmetrically distributed. The main structure of the physical model is shown in Fig. 1.

The structure of a large vertical mill is complex, so its geometric model is constructed after reasonable simplifying the physical model without affecting the calculation accuracy. According to the physical model structure size, the geometric model of the central part of the vertical mill is built. The main part comprises the shell, powder selecting device, rolling device, and air inlet device. The components of the main structure that do not influence the numerical calculation results are discarded to simplify the calculation.

The main working principle of the vertical mill is as follows: the motor drives the grinding disc to rotate through the reducer, and the materials are fed to the grinding disc rotating in the mill by the airlock feeding equipment. Under the action of centrifugal force and friction force, the materials move to the periphery of the grinding disc and enter the grinding roller table. The material retaining ring outside the grinding disc makes the materials form a material layer (i.e., powder grinder). With the rotation of the grinding disc, the grinding roller grinds, presses and grinds the materials on the grinding disc. In this process, some large-particle materials fall into the scraping cavity under the grinding disc through the annular nozzle. The scraping plate of the scraping cavity scrapes the materials to the slag outlet along with the rotation of the grinding disc and then re-feeds them into the vertical mill for grinding through the external circulation equipment (i.e., external circulation of the vertical mill). Due to the action of the circulating fan, the hot air entering the mill passes through the annular nozzle around the grinding disc at a speed of 40~80 m/s to bring the ground materials to the upper part of the grinding machine. The enlarged upper shell of the grinding machine makes the large particle materials fall to the grinding disc for re-grinding due to the slow wind speed. Fine particles enter the dynamic and static classifier together with the airflow for thickness separation. Coarse particles return to the center of the millstone from the blanking cone for grinding again (i.e., the internal circulation of the vertical mill). Then fine particles are discharged out of the mill along with the airflow, and collected by the dust collector to obtain the product.

2.2. A multi-objective optimization approach of large vertical mill based on CFD–DPM

A numerical simulation method is an effective tool for analyzing the gas–solid two-phase flow system. In the CFD–DPM method, the gas phase is regarded as a continuous fluid, and the discrete phase can be solved by tracking the particle trajectory. In this paper, the coarse-grained non-analytical CFD–DPM model is used in the

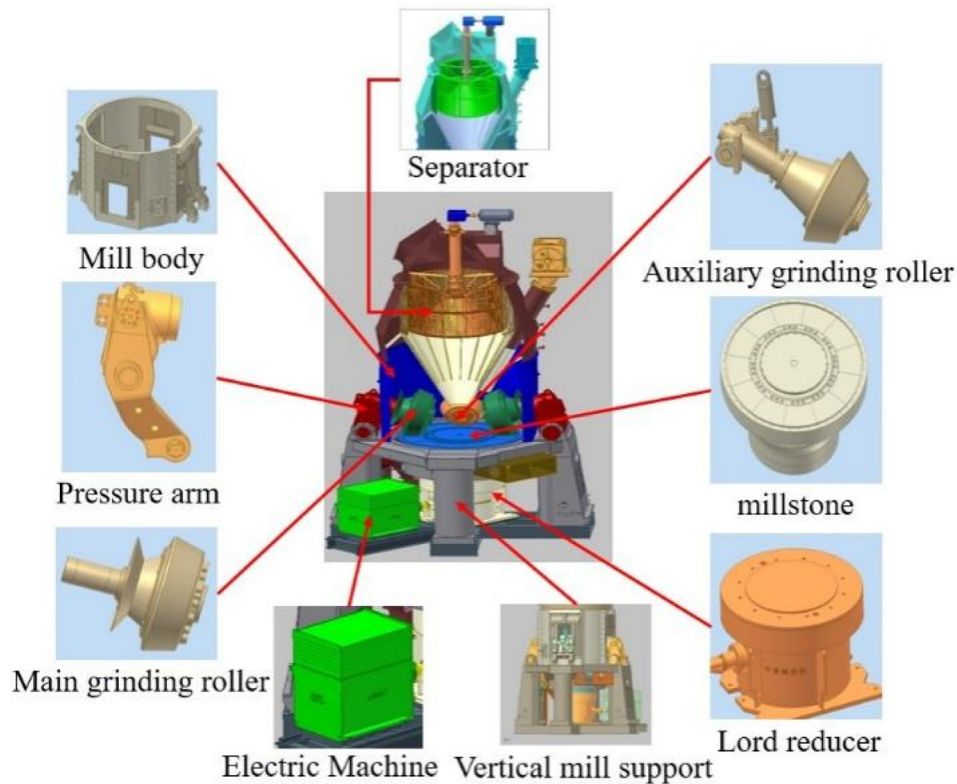


Fig. 1. Structure diagram of key components of vertical mill.

simulation analysis, which reduces the demand for calculation and improves the calculation efficiency.

This study aims to improve the output and production efficiency of a large vertical mill by optimizing its operational parameters. This paper takes a large vertical mill in LGM as the object, a numerical calculation method of particle–fluid coupling system in large vertical mill based on CFD-DPM theory, and a multi-objective optimization method of operating parameters of large vertical mill based on Kriging are proposed. Based on the Kriging surrogate model and genetic algorithm, the optimization framework of operation parameters of a large vertical mill based on Kriging is established. The multi-objective parameter optimization framework of large vertical mill operation is shown in Fig. 2.

A multi-objective optimization process based on CFD-DPM is organized as follows.

Step1:Numerical model of the granular fluid system based on CFD-DPM.

The discrete particle model of computational fluid dynamics is used for numerical simulation and analysis, especially when coupled DPM is used, which involves a large number of particle calculations. To reduce the calculation amount and shorten the calculation cycle, the parcel can effectively improve the calculation efficiency. Finally, the numerical simulation results are compared with the actual values to verify the accuracy of the simulation.

Step2:DOE experimental design and Latin hypercube sampling.

DOE can select the ideal initial sample point with fewer test runs, low cost and short period, and can effectively approximate the unknown objective function. Latin hypercube sampling can make the samples evenly distributed in space.

Step3:Kriging surrogate model and its cross-validation.

The Kriging model is an unbiased estimation model to predict the response of unknown test points through the information of known test points. After forecasting the model, the accuracy and feasibility of the model can be determined by cross-validation.

Step4:Optimization model and an optimization process based on Kriging.

The optimization process is designed based on the Kriging model, and the multi-objective optimization of a large vertical mill is carried out by combining with the NSGA-II algorithm.

3. Numerical model of granular fluid system based on CFD-DPM

3.1. CFD-DPM coupling method

3.1.1. CFD numerical model

As a typical complex particle–fluid system, the structural layout of the nozzle ring, gravity classification zone, and centrifugal separation zone in the internal cavity of a large vertical mill is unclear concerning the fluid field pattern of the gas and solid mixture. It is difficult to accurately describe the coupling relationship between these parameters by using the existing calculation models and methods. This paper uses a coupled CFD-DPM model to simulate the internal flow field of the system numerically.

The standard k - ε turbulence model is a two-equation vortex-viscosity model, mainly used to solve the vortex viscosity coefficient μ_t [15]. The transport equation for turbulent kinetic energy k is solved by equation derivation and the transport equation for dissipation rate ε is obtained by physical reasoning following the structural form of the turbulent kinetic energy equation, and the

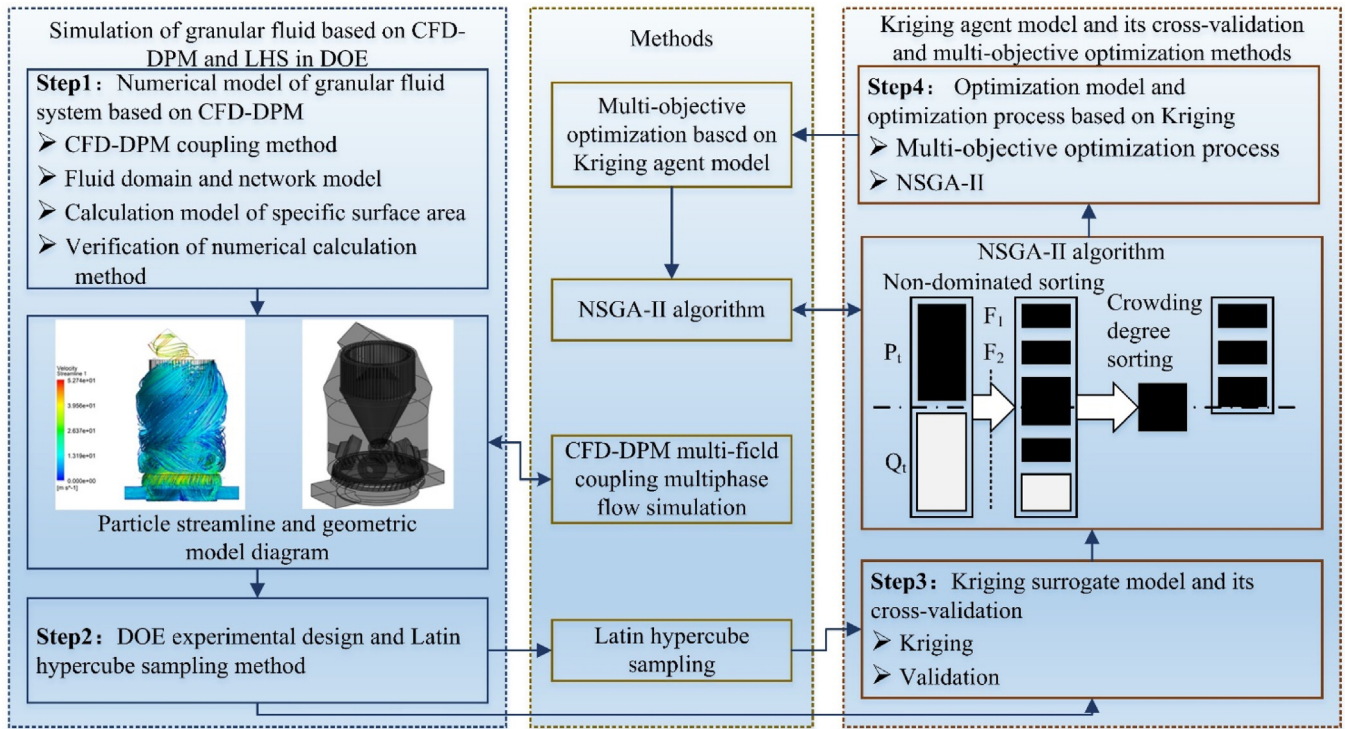


Fig. 2. A multi-objective optimization framework of a large vertical mill based on CFD-DPM.

turbulent kinetic energy and dissipation rate transport equations are expressed as [16].

$$\frac{\partial(\rho k)}{\partial t} + \frac{\partial(\rho u_i \varepsilon)}{\partial x_i} = \frac{\partial}{\partial x_i} \left[\left(\mu + \frac{\mu_t}{\sigma_k} \right) \frac{\partial k}{\partial x_i} \right] + P_k - \rho \varepsilon \quad (1)$$

$$\frac{\partial(\rho \varepsilon)}{\partial t} + \frac{\partial(\rho u_i \varepsilon)}{\partial x_i} = \frac{\partial}{\partial x_i} \left[\left(\mu + \frac{\mu_t}{\sigma_\varepsilon} \right) \frac{\partial \varepsilon}{\partial x_i} \right] + C_{\varepsilon 1} P_k \frac{\varepsilon}{k} - C_{\varepsilon 2} \frac{\varepsilon^2}{k} \quad (2)$$

$$P_k = \mu_t \left(\frac{\partial \bar{u}_i}{\partial x_k} + \frac{\partial \bar{u}_k}{\partial x_i} \right) \frac{\partial \bar{u}_i}{\partial x_k} \quad (3)$$

where μ_i , \bar{u}_i and \bar{u}_k respectively represent the velocity of the fluid mass in Cartesian coordinates, x_i and x_k respectively represent coordinates in different directions, μ is the fluid viscosity, μ_t is turbulent viscosity coefficient, $C_{\varepsilon 1}$ and $C_{\varepsilon 2}$ are usually taken as default constants of 1.44 and 1.92 respectively, the turbulent Prandtl numbers for turbulent kinetic energy and dissipation rate are divided into $\sigma_k = 1.0$, $\sigma_\varepsilon = 1.3$.

3.1.2. DPM theoretical model

The fluid movement with two or more different phases is called multiphase flow. The complex particle–fluid system of a vertical mill is a gas–solid coupled multiphase flow system. Depending on the treatment of the medium, the large-scale particle–fluid system can be described by a two–fluid model or a particle trajectory model. The two–fluid model is suitable for dense–phase particle flow, where the particles are considered as a continuous medium mixed with the gas phase in the Eulerian coordinate system. Unlike dense–phase particle flow, which treats solid particles as fluid-like,

the particle trajectory model treats solid particles as discrete media and examines their motion in the Lagrangian coordinate system. In the case of small volume fractions of particles in the computational fluid domain, the discrete phase model is chosen to avoid the diffusion problem of the numerical solution. The calculation shifts from global averaging to local transients. While the computational accuracy is higher compared to the two–fluid model. Hence the particle trajectory model is used for the numerical analysis.

The particles in the mill are mainly subject to the joint action of gravity, traction, buoyancy and other forces. The forces follow Newton’s second law, and the trajectory of the discrete particles is predicted by integrating the force balance, and the differential equation of motion is written [17].

$$m_p \frac{d\vec{u}_p}{dt} = m_p \frac{\vec{u} - \vec{u}_p}{\tau_r} + m_p \frac{\vec{g}(\rho_p - \rho)}{\rho_p} + \vec{F} \quad (4)$$

Where m_p is the discrete phase particle mass; \vec{u}_p is the particle velocity; \vec{u} is the gas continuous phase velocity; ρ_p is the particle density; ρ is the continuous phase density; \vec{F} is the additional force; $m_p(\vec{u} - \vec{u}_p/\tau_r)$ is the particle drag; τ_r is the particle relaxation time expressed as $\tau_r = (\rho_p d_p^2 / 18\mu) \cdot (24/C_d Re)$, (μ is the gas molecular viscosity; d_p is the particle diameter; C_d is the particle traction coefficient; Re is the relative Reynolds number defined as $Re = [(\rho d_p |\vec{u}_p - \vec{u}|) / \mu]$).

3.1.3. Coarse-grained non-analytical CFD-DPM coupling method

The gas–solid two–phase flow field in the vertical mill cavity was simulated by using the Eulerian–Lagrangian approach to build a multiphase flow model numerically. The vertical mill complex granular–fluid system belongs to the gas–solid coupling multiphase flow system. In the CFD–DPM interphase coupling, The particle trajectory model uses the Eulerian–Lagrangian approach to

treat solid particles as discrete media, and describes their motion by tracking and calculating particle traces in the Lagrangian coordinate system. In the case of small particle volume fraction in the computational fluid domain, the discrete phase model can avoid the diffusion problem of numerical solution, and the calculation shifts from the overall average to the local instantaneous. The gas flow inside the cavity is non-viscous gas non-constant flow (i.e., non-stationary flow), and the gas phase is considered as a continuous medium in the Eulerian coordinate system [18,19]. Discrete media is in the Lagrangian coordinate system, adopting the DPM model. The movement of particles was described by tracking and calculating their trajectories. The two phases are coupled, the exchange of momentum, mass and energy between discrete and continuous phases, and the continuous phase is solved for the turbulent non-constant Reynolds-averaged Navier-Stokes equations based on the solver. When the iterations converge, the discrete phase is introduced to solve the particle trajectory equations, and the particle source term of the continuous phase is updated for the next iteration until the coupling converges. Fig. 3 shows the flow chart of the coupling calculation.

When using coupled DPMs in numerical simulations, the mass flow rate of particle injection is often a necessary and relevant input parameter. It determines the absolute value of the DPM source, as the mass flow rate can be converted into the number of particles injected per unit of time. Faced with the problem that the complex particle-fluid system is stuck or even unable to calculate. When a large number of particles are involved in the system, the parcel can reduce the calculation amount and shorten the calculation cycle. Parcel represents a fraction of the total continuous mass flow rate (in a stable trace) or a fraction of the total mass flow rate released in a time step. Because it has a specific particle size, the calculation treats it as a coarse-grained model whose fluid flow

trajectory uses a relaxation time appropriate to the individual particles (relaxation time is the ratio of particle momentum to drag) and helps converge [20]. Therefore, no single parcel will significantly affect on the flow, and sufficient parcels should be arranged to generate statistical samples to represent the whole range of particle behavior.

3.2. Fluid domain and network model

The numerical simulation method is used to solve the flow problem. In addition to the differential equations used to describe the fluid motion, it is also necessary to determine its definite solution conditions. The definite solution conditions of unsteady flow are composed of boundary and initial conditions. The gas phase inlet boundary condition is set to velocity inlet with a single inlet area of 2.34 m², and the outlet boundary type is set to free outlet (outflow). The discrete phase particles are generated from the surface of the grinding disc. The tracking particles are calcium carbonate with a density of 2 800~3 400 kg/m³ taking 3 000 kg/m³. The solid phase inlet boundary is defined as a trap, the particle injector type is a model surface jet source with a mass flow rate of 25 kg/s (The actual feeding speed of the large vertical mill is 90 t/h, and the mass flow rate of the particle syringe model surface injection source is set to 25 kg/s after unit conversion, which is the model condition setting in the simulation system.) , and the particle outlet boundary is defined as an escape. The parcel number in the DPM model is selected in model settings, not limited by the actual particle number. Parcel is to collect particles for calculation, in the face of complex particles-fluid system numerical calculation processing is large, there is a problem that the calculation process is stuck or even unable to calculate, especially when a large number of particles are involved in the system, the amount of calculation

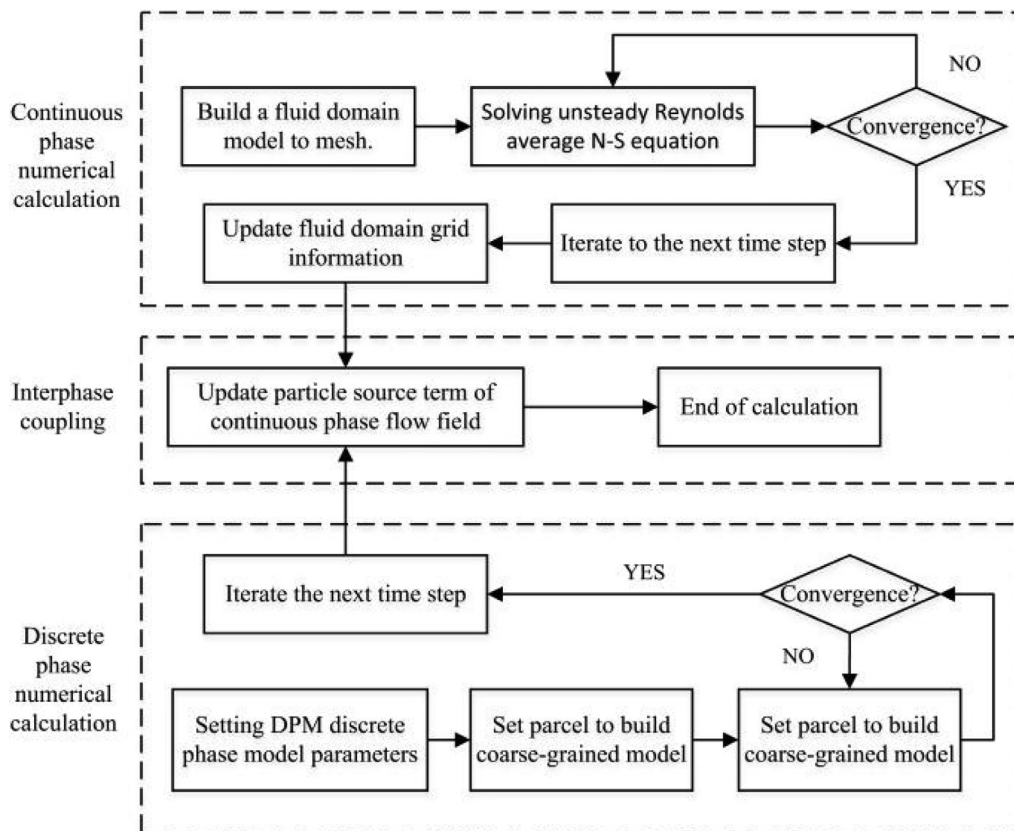


Fig. 3. Flow chart of CFD-DPM coupling calculation.

can be reduced and the calculation cycle is shortened with the help of Parcel. Parcel represents a portion of the total continuous mass flow (in a steady trace) or a portion of the total mass flow released in a time step. We select constant-mass, and define a parcel mass as 2.5×10^{-5} kg. Fig. 4 (a) shows the flow field domain model. The number of ejected particles per second is $25/2.5 \times 10^{-5}$.

The solution method uses an implicit pressure–velocity coupled solution based on a pressure solver, with a low number of iterative steps and a fast convergence rate. In the interphase coupling calculation, the discrete phase and the continuous phase interact and transfer among momentum, mass and energy. Each time step is solved iteratively. The calculation is finished when the two-phase calculation results reach the convergence standard. The Green-Gauss Cell Based algorithm was selected for the gradient algorithm. The second-order format is selected for the pressure phase difference format., The spatial discrete schemes are all calculated by the second-order upwind scheme. The relaxation factor adopts the default value to ensure the stability and convergence of the calculation.

Due to the complex spatial structure of the model, a partitioned meshing method is used to ensure the quality of the meshing, with different regions being divided into structured or unstructured meshes depending on the structure and calculation accuracy requirements, with the regions connected by interfaces. The mesh quality is reflected in the rationality of the mesh geometry. The degree of mesh distortion will reduce the accuracy of numerical calculations. In order to improve the accuracy of the calculation, we ensure both the reasonable division of the mesh and a reasonable transition of the fluid between the guide blade and the rotor blade. The rotor blade and the guide blade around the mesh encrypt the processing. Fig. 4 (b) shows the Fluid domain grid model.

3.3. Calculation model of specific surface area

Specific surface area is another important indicator to measure the fineness of powder products, usually divided into volume-specific surface area $S_v(\text{m}^2/\text{m}^3)$ and mass-specific surface area $S_w(\text{m}^2/\text{kg}; \text{m}^2/\text{g})$. We have $S_v = \rho_p S_w$ (ρ_p for particle density) correspondence, expressed as a unit volume or mass of powder particles with a total surface area. The national standard value for silicate

cement specific surface area is no $<300 \text{ m}^2/\text{kg}$. The larger the value, the finer the powder particles.

To count the number of particles in different particle size ranges, we can describe the distribution of powder particle sizes by tabulating or making frequent and cumulative distribution diagrams and also by using analytical mathematical functions to generalise and describe the distribution pattern of powder particle sizes.

The Rosin-Rammler distribution function is based on the study of probability and statistical theory, through the cement, coal powder and other fine powder material crushing experiments and summed up the exponential function. In line with the R-R distribution of the particle group, sieve residual cumulative distribution function can usually be expressed as [21].

$$R(D) = 100 \exp \left[-(D/D_e)^n \right] (\%) \tag{5}$$

where $R(D)$ represents the cumulative mass percentage of the sieve residue when the particle size is D . When $D = D_e$, the cumulative mass percentage of the sieve residue $R(D_e) = 100/e\% = 0.368$, the corresponding particle size is the characteristic particle size of the particle population D_e , the characteristic particle size can roughly reflect the coarseness of the powder; n is the uniformity coefficient, which is used to characterize the width of the particle size distribution range.

For theoretical analysis, the exponential function $R(D)$ was linearized by taking twice logarithms.

$$\lg [\lg(100/R(D))] = n \lg D + C \tag{6}$$

$$C = \lg \lg e - n \lg D_e$$

In the X-Y coordinate system, such that $Y = \lg [\lg(100/R(D))]$, $X = \lg D$, the Rosin-Rammler equation was transformed into a linear (or approximately linear) solution. Linear regression analysis was used to obtain the slope n , the intercept C , and the linear correlation coefficient r . The characteristic particle size D_e was obtained through the intercept C .

When a powder can be expressed as a function, an analytical solution for a specific surface area can be obtained. By integrating the frequency distribution function, the particle accumulation distribution function can be obtained for any $D_i \sim D_{i+1}$ range. By deriving the particle under-screen accumulation distribution function, the frequency distribution function can be obtained

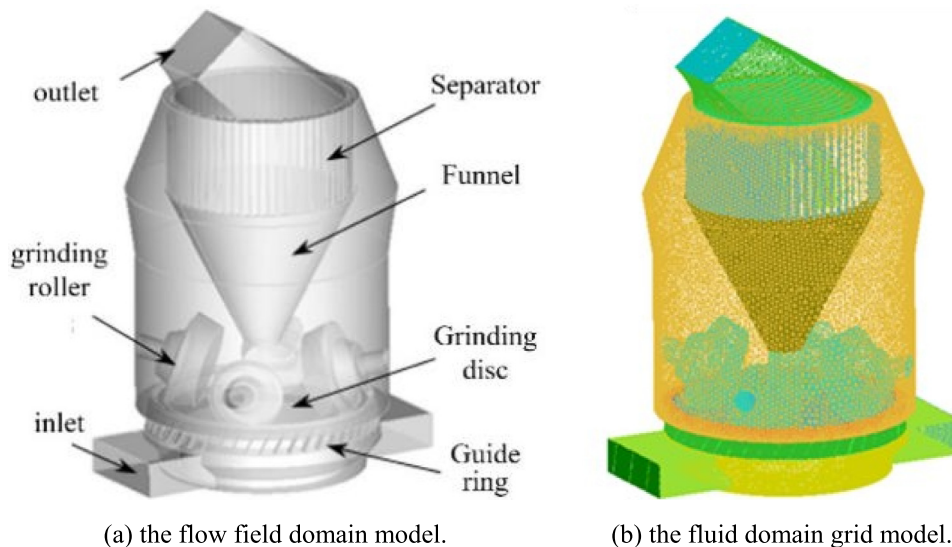


Fig. 4. Vertical mill flow field.

$$f(D) = [1 - R(D)]^n = (n/D_e^n) e^{-(D/D_e)^n} D^{n-1} \quad (7)$$

The integration of the frequency function for particle size D (equivalent diameter of the specific surface area of the particle) in the interval $(0 \sim \infty)$ gives

$$S_v = \rho_p S_w = (\varphi_{sv}/D_e) \int_0^\infty (D^{n-2}/D_e^{n-1}) e^{-(D/D_e)^n} dD \quad (8)$$

where φ_{sv} is the specific surface area shape factor.

The formula for calculating the specific surface area of the Rosin-Rammler distribution function is obtained by simplifying the integral and has an approximate solution when $n = 0.7 \sim 2.5$ (positive and negative errors $< 2.5\%$).

$$S_v = \rho_p S_w = 1.065(\varphi_{sv}/D_e) \exp(1.795/n^2) \quad (9)$$

3.4. Validation of numerical calculation method

Following the above method, numerical calculations are carried out, and the results are compared with the experimental vertical mill operation data. The experimental data in this paper comes from the developed mining equipment industrial internet platform, which has realized the whole process condition monitoring of the large vertical mill. The vertical grinding condition is set to the speed of the powder separator 110 r/min, the inlet and outlet pressure difference is 3 523 Pa, and the system air volume is 415.1 m³/h. A comparison of the experimental data with the numerical calculation data is shown in Table 1.

Based on the above theory, numerical simulations were carried out with the same operating parameters. The distribution of particles escaping from the outlet is counted, and the analytical solution of its specific surface area is 402.33 m²/kg. The relative error with the experimental value is 3.08%. The two primary sources of errors are the difference between the simplified calculation model and the actual physical model, and the approximation error in the chosen specific surface area calculation model. The experiments and simulations are in good agreement and can be used with the numerical calculation of the sampling points in establishing the proxy model.

3.5. DOE experimental design and Latin hypercube sampling

Design of Experiments (DOE) is a mathematical and statistical method widely used in product development, quality control, process optimization and other areas. To construct the surrogate model, DOE is the first step. The two purposes of DOE include (1) selecting the ideal initial sample points with fewer runs, lower cost, and shorter cycle time, and (2) effectively predicting the unknown objective function. The choice of DOE directly affects the construction cost of the approximation model and the accuracy of the approximation. Common DOEs are Latin Hypercube design (LHD), Optimal Latin Hypercube design (Opt LHD), Full Factorial Design (FFD), Fractional Factorial Design (FFD), Orthogonal Experimental Design (OED) and Central Composite Design (CCD), etc. [22] To obtain the desired experimental results, the selection of the initial sample points is essential. A small number of initial sample points will reduce the approximation accuracy of the proxy model. At the same time, too many sample points will result in repeated calculations that do not reflect the efficiency of the proxy

Table 1
Comparison of experimental data with numerically calculated data.

Working conditions	Measured values	Simulation calculations
Specific surface area m ² /kg	415.1	402.33

model in the optimization design process. Sample points should be evenly distributed throughout the design space to avoid the superposition of sample points within the same level. In this paper, Opt LHD is used for sampling.

4. Kriging surrogate model and its cross-validation

4.1. Kriging surrogate model

Kriging method [23] is a regression algorithm for spatial modeling and prediction of random processes according to covariance function, and it is an unbiased estimation model with the smallest variance. A stochastic process represents the relationship between the objective function and design variables. The response $\hat{y}(x)$ of unknown sample points can be predicted by a linear combination of responses of known sample points. The Kriging has the following equation.

$$\hat{y}(x) = f(x) + Z(x) \quad (10)$$

where $f(x)$ is a known function of x and represents a global approximate simulation, $Z(x)$ is a stochastic process model with a mean of 0 and variance σ^2 created by quantifying data observations and data correlations, and x represents the design variables.

The covariance of $Z(x)$ is:

$$\text{cov}[Z(\mathbf{x}_i), Z(\mathbf{x}_j)] = \sigma^2 \prod_{k=1}^n R_k(\theta_k, d_k) \quad (11)$$

where θ_k is the model parameters to be determined, n is the number of design variables, d_k is the k dimensional distance between sample points, and $R_k(\theta_k, d_k)$ is the correlation function. Commonly used correlation functions are: Gaussian function, exponential function, spline function, linear function, etc.

4.2. Leave-One-Out Cross-Validation

In this paper, we use Leave-One-Out cross-validation [24] to assess the accuracy of the initial kriging model, as this procedure allows us to evaluate the accuracy of the model without sampling any points other than those used to fit the model. The basic principle of Leave-One-Out cross-validation is to omit an observation $y(\mathbf{x}^{(i)})$ and make a prediction based on only $n-1$ sampled points. We can then obtain a cross-validated observation prediction, e.g. $\hat{y}_{-i}(\mathbf{x}^{(i)})$, and a cross-validated standard error of the prediction, e.g. $\hat{s}_{-i}(\mathbf{x}^{(i)})$. The subscript $-i$ indicates that the observation i was not used in building the kriging model. These two quantities can be used to calculate standard amounts to determine whether the initial kriging model is valid.

$$Sr = [y(\mathbf{x}^{(i)}) - \hat{y}_{-i}(\mathbf{x}^{(i)}) / \hat{s}_{-i}(\mathbf{x}^{(i)})] \quad (12)$$

where Sr is called the standardized cross-validation residual. If Sr lies in the interval $[-3, +3]$ and interval $[-80, +80]$, the confidence level of the kriging model is approximately 99.7%, which means that the model is valid. We selected 31 samples by LHS code to build the initial kriging model in this case.

Fig. 5 shows the results of the diagnostic tests for the initial kriging model. In Fig. 5, the observed versus cross-validated predictions are plotted. The points will lie on the 45° line if the model is good. As shown in Fig. 5, the 31 samples are largely distributed around the 45° line. In Fig. 5 (b) and (d), it is more evident that the standardized cross-validation residuals for all 31 samples are in the interval $[-1.5, +1.5]$ and interval $[-40, +40]$, respectively, so the initial kriging model is satisfactory.

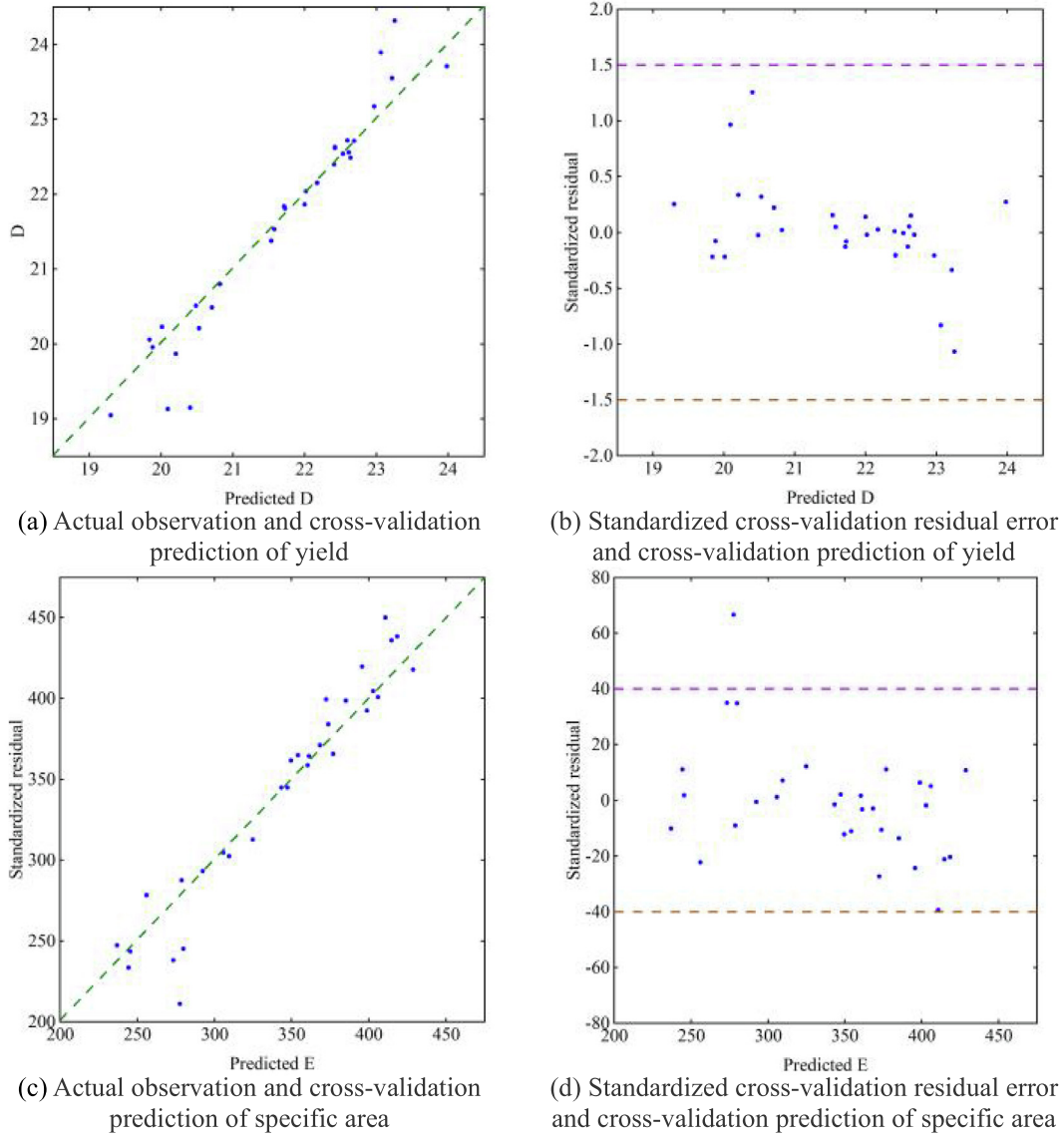


Fig. 5. Diagnostic tests for the Kriging model.

5. Multi-objective optimization process based on Kriging

5.1. Multi-objective optimization process

In multi-objective optimization problems, there are usually conflicting relationships between the objective functions and no individual solution can optimize all the objectives at the same time, with the optimal solution being the solution set. The mathematical model is shown below.

$$\min \mathbf{F}(x) = [f_1(x), f_2(x), \dots, f_m(x)]^T \quad (13)$$

$$s.t. \begin{cases} g_i(x) \leq 0, & i = 1, \dots, p \\ h_j(x) = 0, & j = 1, \dots, q \\ l_k \leq x_k \leq u_k, & k = 1, \dots, n \end{cases} \quad (14)$$

where: $g_i(x) \leq 0$ is the inequality constraint, $h_j(x) = 0$ is the equation constraint, $l_k \leq x_k \leq u_k$ represents the upper and lower bounds of the variables x_k are l_k and u_k respectively, and the decision vector x is sought in the decision space such that $F(x)$ is minimized when the above two types of constraints are satisfied. In this experiment, the objective functions were yield and specific surface area, respec-

tively. The yield and specific surface area were sought as the maximum value. Therefore, in function setting process, the $f(x)$ representing yield and specific surface area were taken as a negative value, and the opposite number was taken after the minimum value was obtained as the maximum value of these two objective functions.

Fig. 6 shows the multi-objective optimization framework for large vertical mill operating parameters. The specific optimization process is as follows.

Step 1 Sampling using the optimal Latin hypercube method to obtain a uniformly distributed sample.

Step 2 Calculate a Kriging surrogate model between the design variables and the objective function by coupling CFD-DPM to the sample.

Step 3 Determine whether the combined surrogate model meets the accuracy requirements; if it does, proceed to the next step; if it does not, return to step 1.

Step 4 Optimization based on the combined surrogate model, using the NSGA-II algorithm on the MATLAB platform to obtain optimization results.

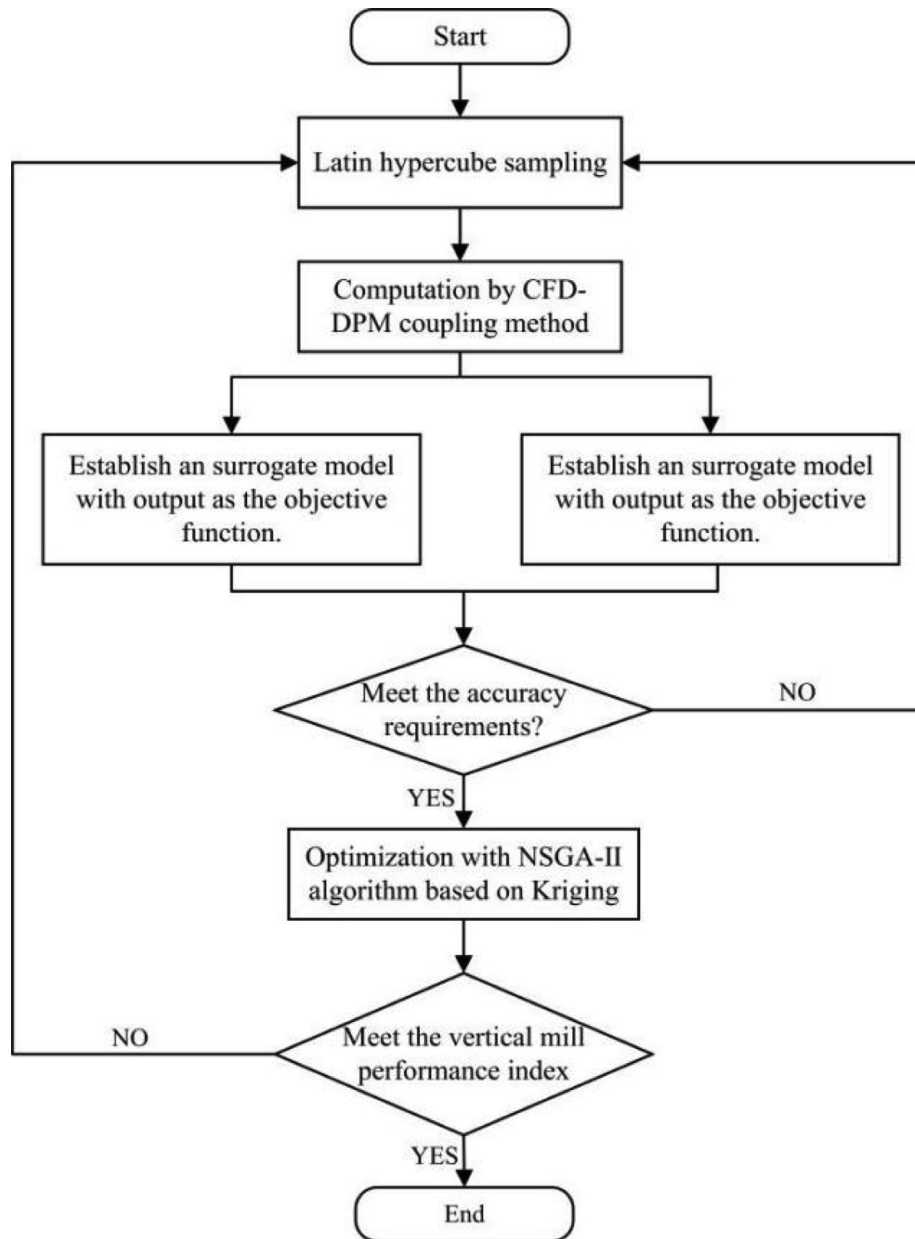


Fig. 6. Multi-objective optimization framework for large vertical mill operating parameters.

Step 5 Determine whether the optimization result meets the performance index requirements of the vertical mill. If so, the optimization is completed; if not, return to step 1.

5.2. Non-dominated sorting genetic Algorithm-II(NSGA-II)

The multi-objective optimization of vertical mill operating parameters is a complex problem with nonlinearities multimodality and discontinuities. CFD-DPM can obtain the value of the objective function, but derivative (gradient) information is not easily available. Genetic algorithms based on natural selection theory use only the value of the objective function, with no gradient information. This feature makes genetic algorithms an effective search mechanism for running parametric multi-objective optimization [25].

Fig. 7 shows the general process of the genetic algorithm. Firstly, initialize the population. Order all individuals in a non-dominated relationship and assign a fitness value. Then, the next generation population is generated by selection, crossover, and mutation operators. The size is recorded as N .

The new population is merged with the parent, and then a series of non-dominated sets ($F(1)$, $F(2)$, ..., $F(n)$) are generated by non-dominated sorting. The crowding degree is calculated, and appropriate individuals are selected to form the new parent population. If $F(1)$ is less than N , the next dominant set $F(2)$ is added to the new parent population until the population size exceeds N , and the crowding degree of the finally added non-dominant set individuals is sorted, and the appropriate individuals are selected to make the number of the new parent population reach n . Then a new offspring population is generated by genetic operators.

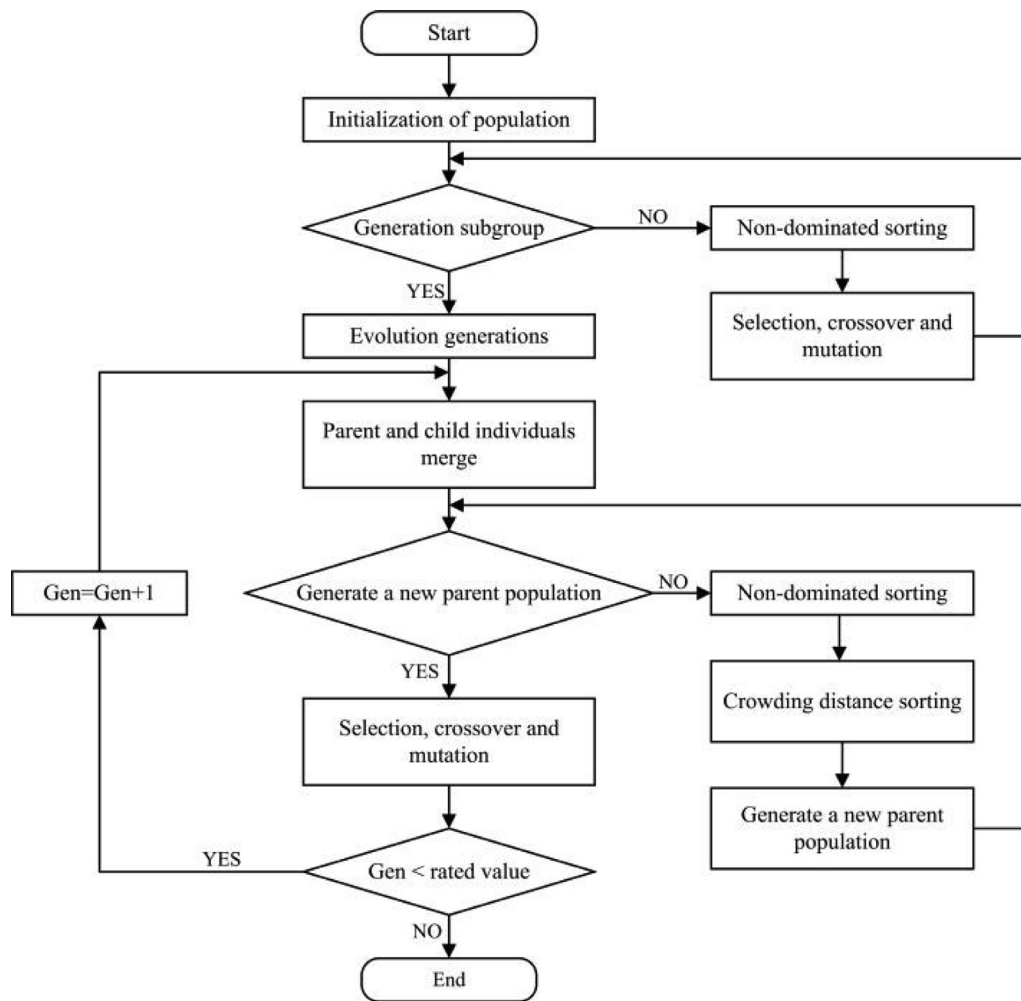


Fig. 7. Overall flow chart of NSGA-II algorithm.

6. Case study

The proposed Kriging model is applied to the multi-objective optimization design of vertical mill operating parameters and compared with the simulation results to verify the practical effect of the proposed Kriging model on the optimization of vertical mill parameters.

6.1. Description of the problem

The complex particle–fluid system has many monitoring operating points and operating parameters. There are many parameters in the operation of a large vertical mill, such as feed rate, air intake rate, rotation speed, powder output, water consumption, powder particle size, etc., and the coupling relationship among the parameters is highly complex. The influence mechanism of each operating parameter on the system flow field and the result of powder separation is unknown. Through the analysis of the numerical calculation results, it is known that the inlet air speed, the rotational speed of the powder separator, and the outlet temperature of the vertical mill are the key parameters that mainly affect the production capacity, the production efficiency, and the production quality of the equipment.

The inlet air velocity is recorded as A. The fineness of the powder is an important indicator of the quality of the finished product. The powder particles can be collected as qualified products only

after gravity and centrifugal classification. The inlet air velocity is the main parameter that determines the particle size of the centrifugal classification cut, which directly affects the powder’s particle size distribution and the fineness of the finished product. According to the actual physical model, the air velocity can be set at the 12 ~ 15 m/s.

The rotating speed of the classifier is recorded as B. The rotating speed of the powder separator is another main parameter that determines the particle size of centrifugal classification cutting. The value changes have the most obvious influence on the surface area of the finished product. According to the running power of the powder separator, the rotating speed is set in the range of 80 ~ 150 r/min.

The outlet temperature of the vertical mill is recorded as C. With a specific air volume and speed of the separator, the outlet temperature affects the circulating load of the equipment. When the load decreases, the outlet temperature rises, and the grinding efficiency increases. Temperature also affects the pressure distribution in the mill. Keep the inlet temperature unchanged, and set the outlet temperature according to the temperature difference between the inlet and the outlet, with the value ranging from 80 ~ 120°C.

The production (kg/s) and the surface area of the finished product (m²/kg), which can evaluate the production efficiency and quality of a large vertical mill, are the optimization targets. Note as D and E, respectively. A set of operating parameters represented

by each initial sample point were taken as independent working conditions. A numerical model of particle–fluid–temperature multi-physical field coupling was established for simulation calculation. Based on the simulation results, the values of D for the production rate and E for the fineness of the finished product for different working conditions of the large vertical mill are obtained. The results are used as the initial same points' response values to construct the proxy model.

In summary, the multi-objective optimization problem for vertical mill operating parameters can be described as presented in Table 2.

6.2. Analysis of experimental design results

Pareto diagrams, main effect plots and interaction effect plots were produced from the experiment results to examine the response of the two objectives of yield and specific surface area to the experimental design variables for analysis.

Pareto diagrams, in the form of a percentage chart according to the test results, intuitively reflects the influence and contribution degree of each factor to each response after sample fitting, also known as factor contribution rate chart. In Pareto diagrams, design variables are marked in blue for positive relationships with response values and in red for negative relationships. Fig. 8 gives a Pareto diagram of the response of each output. The yield is expressed as D. The image shows that the inlet air velocity A and the outlet temperature C have a positive effect on the yield D. The speed of the separator B has a negative effect on the yield D, with A and B contributing the most to the yield D, with C having a smaller effect on the yield D. The surface area is expressed as E,

Table 2
Optimization notes.

	Function/variable	Description	Quantity
Minimize	-D & -E	Negative output and negative specific surface of the product	-
Design variable	[A, B, C]	Air inlet velocity, Outlet temperature, Speed of the separator	[15, 110, 100]
Constraint condition	12 < A < 25 80 < B < 150 80 < C < 120		

with the greatest contribution of factor B, the second influence of factor A, and the lesser influence of factor C. Factors B and C have a positive effect on the surface area, while factor A has a negative effect.

In multilevel, multi-factor experimental designs, the Main Effects Graph is used to describe the degree of influence of a single factor on the response at each level. The larger the value of the main effect indicates, the greater the influence of the factor on the response, as shown in Fig. 9 that is, the main effects graph of inputs A, B, C and responses D and E. From the image, the effect of each input and each corresponding effect between the same Pareto is consistent, with inputs A and B having a greater impact on responses D and E, and C having a smaller effect on the two responses.

The interaction effect diagram reflects the relationship and influence of the interaction between two factors on the response. The curves are the main principle effect diagrams of one factor at different levels of the other factor on the response. Combining the Pareto diagram with the main effect diagram, the interaction between input A, which has the greatest effect on response D, and input B, which has the greatest effect on response E, and the other inputs are analyzed, as shown in Fig. 10. This is the interaction effect diagram for each response's main effect factors. The degree of non-parallelism reflects the strength of the interaction. From the image, we can see that for response D, there is an interaction between its main influencing factors; for response E, there is an interaction between B-C and B-A, and the interaction effect is stronger.

6.3. Analysis of optimization results

Optimize the objective functions D and E, and the Pareto optimal solution set is obtained. The EDM post-processing module receives the distribution of corresponding solutions between design factors and output responses. The distribution of the corresponding solutions between the design factor and the output response is obtained by the EDM post-processing block, as shown in Fig. 11 and Fig. 12, respectively, the Pareto solution set EDM plots of input and response.

Due to the contradictory nature of the two objectives, achieving the optimum solution for the output and finished product surface area is impossible. According to the optimization results, under the condition that both the specific surface area and the output can get

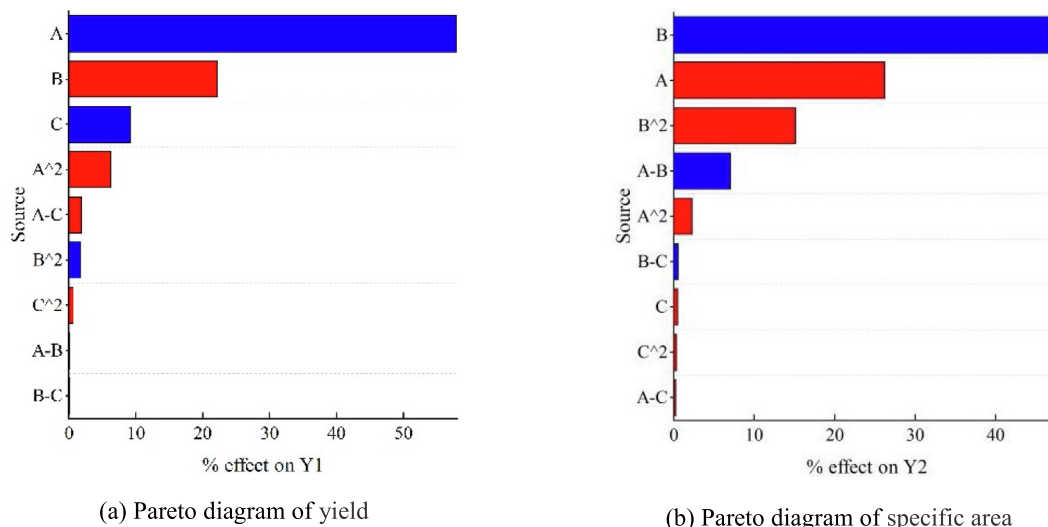


Fig. 8. Pareto diagram of the output response.

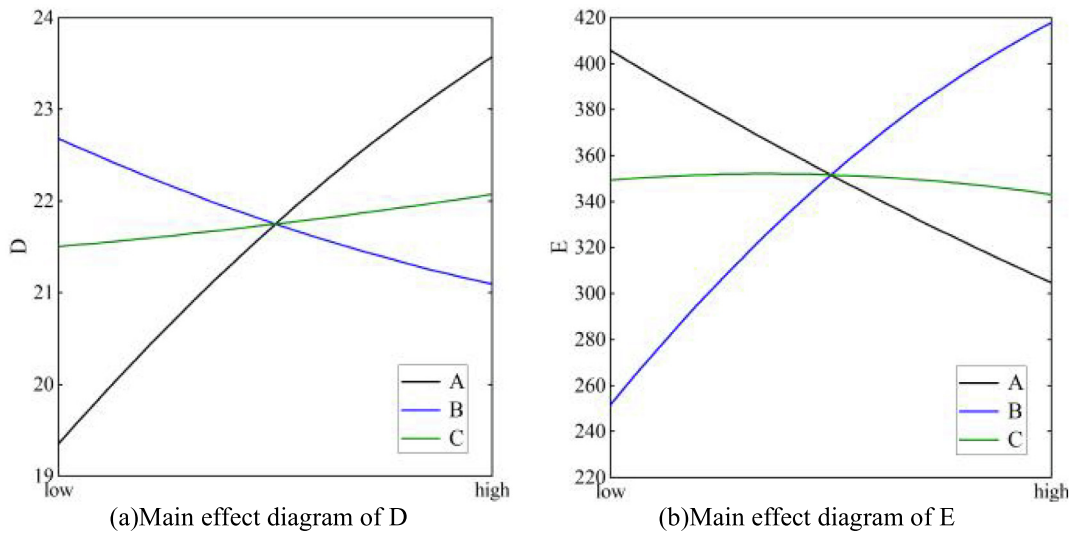


Fig. 9. Main effect diagram of target response.

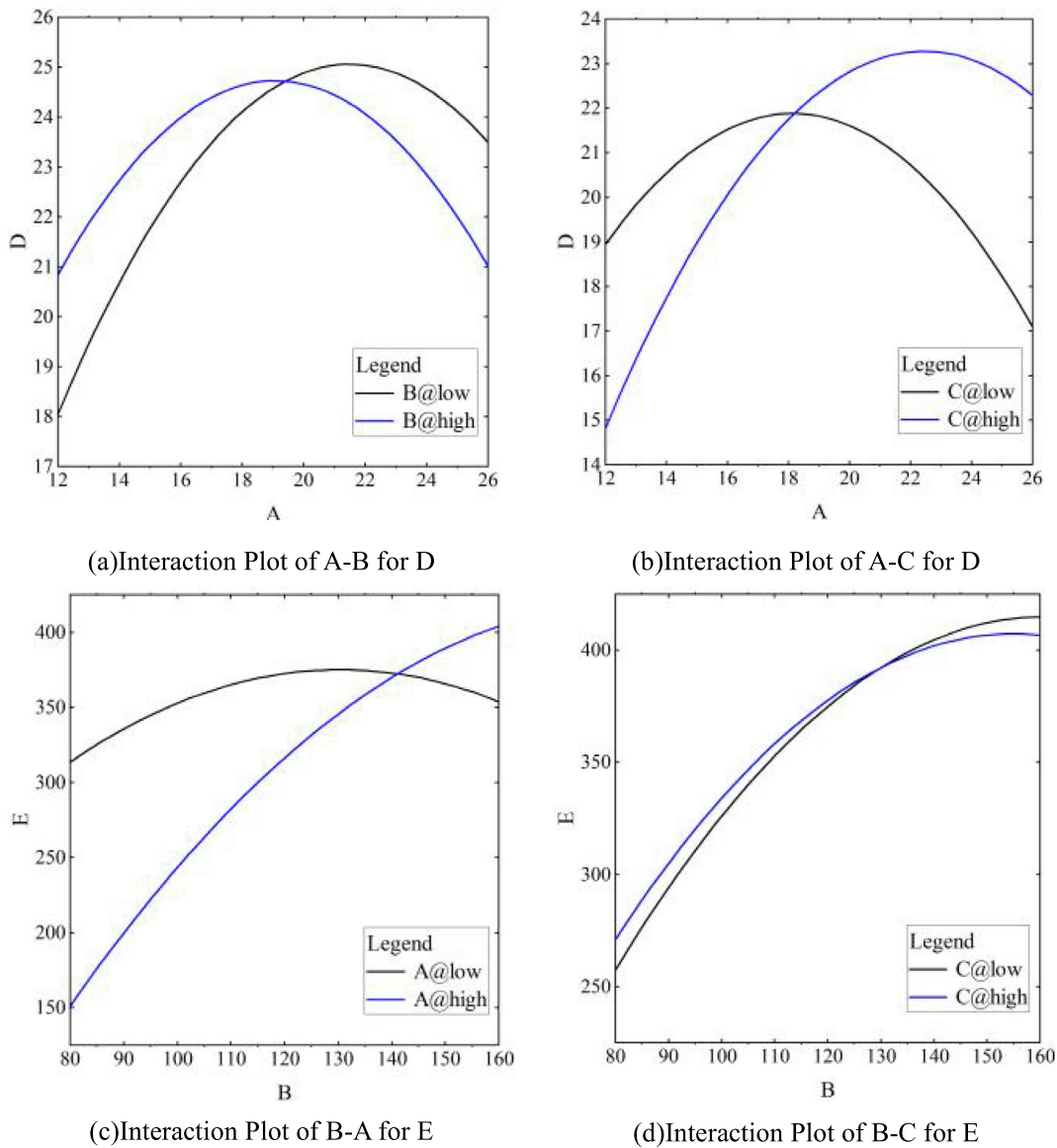


Fig. 10. Interaction effect diagram.

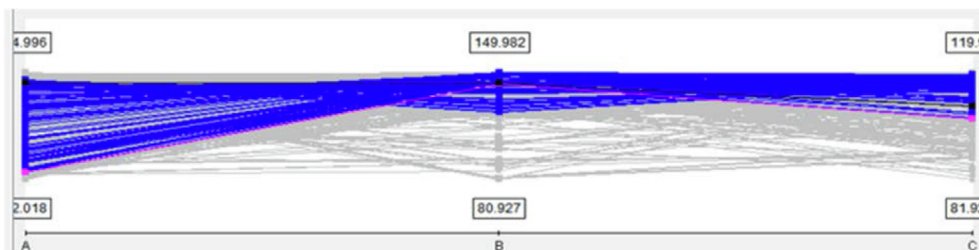


Fig. 11. Pareto solution set EDM plot of design variables.

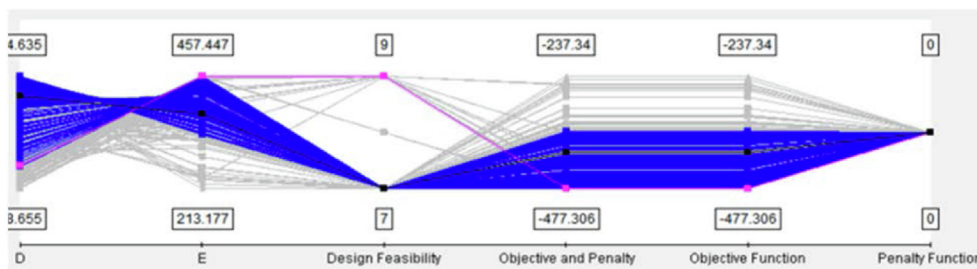


Fig. 12. Output Pareto deset EDM plot of response.

Table 3
Comparison of initial working conditions and optimization results.

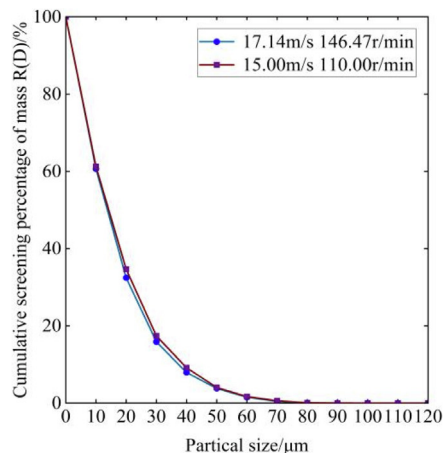
Input and response	Initial value	Optimization results	Amount of change
Wind speed A (m/s)	15.00	17.14	14.27%
Rotational speed B (r/min)	110.00	146.47	33.15%
Outlet temperature C (°C)	100.00	107.78	7.78%
Output D (kg/s)	20.60	21.70	5.34%
Specific surface area E (m ² /kg)	382.33	417.00	9.07%

large values, a group of solutions is selected from the Pareto optimal solution set and used as compromise solutions. The comparison of input and response before and after optimization is shown in Table 3. Increasing the speed of the separator, the inlet air speed and the outlet temperature in the feasible interval can effectively improve the output and fineness of the finished product, and the selected optimal solution increases the output by 5.34%

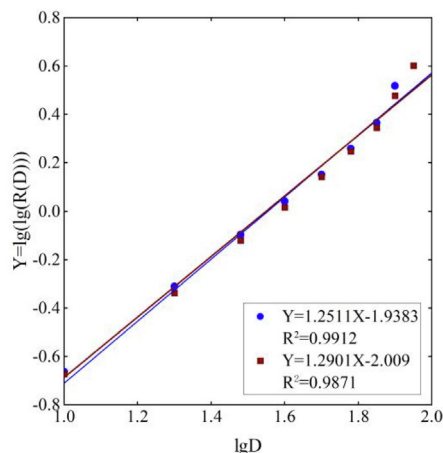
and the specific surface area of the finished product by 9.07%. After determining the optimization solution, the values of the parameters were entered into a numerical calculation model for simulation.

6.4. Validation of optimization results

According to the output optimization results, we change the parameters for numerical simulation. The inlet air speed was set to 17.14 m/s, the separator speed was set to 146.47 m/s, and the outlet temperature was set to 107.78 °C. All other parameters were kept constant. The massive escaping of particles from the outlet was analysed in Fluent. The ratio of the powder mass to the calculation time yield D (kg/s) was calculated to be 22.01 kg/s. By generating a discrete phase sample report, the cumulative sieve residue distribution curve of particles under the corresponding working conditions and the R-R double logarithm fitting particle size distribution function are obtained, as shown in Fig. 13.



(a) Cumulative sieve residue distribution curve of particles



(b) The R-R double logarithm fitting particle size distribution function

Fig. 13. Cumulative sieve residual distribution and R-R fitting curves for standard and optimized working conditions.

Table 4
Validation of simulation optimization results.

Optimization objectives	Optimization results	Simulation results	Relative error
Output D (kg/s)	21.70	22.01	1.43%
Specific surface area E (m ² /kg)	417.00	425.41	2.02%

According to the linear regression fitting result $Y = 1.2511X - 1.9383$, $R^2 = 0.9912$, the characteristic particle size can be calculated from Equation 2–23, D_e is 18.19 μm , the characteristic particle size is brought into Equation (9) to obtain the calculated specific surface area is 425.41 m²/kg, as shown in Table 4 that is the comparison between the simulated and predicted values, with the maximum relative error of 2.02%, which is a high reliability, indicating that it is feasible to establish surrogate model instead of numerical simulation calculation.

7. Conclusion

The numerical simulation of large vertical mill involves the complex coupling of large-scale particles and fluids, which has a large amount of calculation and a long calculation cycle, which cannot meet the requirements of optimization calculation, and there is a problem that the correlation mechanism between key operating parameters and multi-physics morphology is not clear, and the optimization efficiency of equipment operating parameters can be improved with the help of approximate models.

For the optimization of operating parameters of large vertical mills, this paper determines the optimization design variables and multiple optimization objectives according to the modeling and numerical simulation requirements of large vertical mills, takes the three key process parameters of vertical mill inlet air speed, powder separator speed and outlet temperature as the optimization design variables, takes the output and the specific surface area of the finished powder as the optimization goals, and applies the optimal Latin hypercube experimental design method to randomly select the initial sample points in the design space.

In this paper, a numerical calculation method for internal particle–fluid coupling system of large vertical mills based on CFD-DPM theory and a multi-objective optimization method for operating parameters of large vertical mills based on kriging are proposed, and the response value of sample points is calculated by multi-physics coupling simulation technology, and a Kriging surrogate model between optimization targets and influencing factors is constructed to study the optimization of operating parameters of vertical mills. The NSGA-II was used to update the surrogate model and obtain the optimal solution, and the optimized operating parameters increased the vertical mill yield by 5.34% and the specific surface area by 9.07%. According to the optimization results, the powder selection efficiency of the large vertical mill was optimized, and the maximum relative error between the simulated value and the optimized value was obtained by numerical calculation, which verified the superiority of the optimization method of the large vertical mill for performance improvement, so as to realize the application of the operation parameters and key components optimization design of the large vertical mill in engineering.

Declaration of Competing Interest

The authors declare that they have no known competing financial interests or personal relationships that could have appeared to influence the work reported in this paper.

Acknowledgements

This research was supported by the National Science Foundation of China (Grant No. 52175256) and the Henan Provincial Department of Science and Technology Research Project (212102210049).

References

- [1] K. Holmberg, P. Kivikytö-Reponen, P. Härkisaari, K. Valtonen, A. Erdemir, Global energy consumption due to friction and wear in the mining industry, *Tribol. Int.* 115 (2017) 116–139.
- [2] R.A.C. Varas, M.A. Valenzuela, Empirical Determination of the Effect of Lifter Wear in Mill Power for Dry Grinding, *IEEE Trans. Ind. Appl.* 53 (3) (2017).
- [3] D. Altun, H. Benzer, N. Aydoğan, C. Gerold, Operational parameters affecting the vertical roller mill performance, *Miner. Eng.* 103–104 (2017) 67–71.
- [4] A. Elkaroui, S.B.H. Ayeche, M.H. Gazzah, N.M. Saïd, G.L. Palec, Numerical study of local entropy generation in a heated turbulent plane jet developing in a co-flowing stream, *App. Math. Model.* 62 (2018) 605–628.
- [5] C. Bhasker, Numerical simulation of turbulent flow in complex geometries used in power plants, *Adv. Eng. Softw.* 33 (2) (2002) 71–83.
- [6] P. Kozłub, A. Klimanek, R.A. Biłalecki, W.P. Adamczyk, Numerical simulation of a dense solid particle flow inside a cyclone separator using the hybrid Euler-Lagrange approach, *Particuology* 31 (2017) 170–180.
- [7] H.B. Vuthaluru, V.K. Pareek, R. Vuthaluru, Multiphase flow simulation of a simplified coal pulveriser, *Fuel Process. Technol.* 86 (11) (2005) 1195–1205.
- [8] H.J. Dou, X.T. Chai, W.H. Nie, Numerical Study of the Flow Field in a Vertical Roller Mill, *Appl. Mech. Mater.* 52–54 (2011) 659–663.
- [9] P. Toneva, K.-E. Wirth, W. Peukert, Grinding in an air classifier mill – Part II: Characterisation of the two-phase flow, *Powder Technol.* 211 (1) (2011) 28–37.
- [10] Y. Mori, C.-Y. Wu, M. Sakai, Validation study on a scaling law model of the DEM in industrial gas-solid flows, *Powder Technol.* 343 (2019) 101–112.
- [11] M. Zamani, S. Seddighi, H.R. Nazif, Erosion of natural gas elbows due to rotating particles in turbulent gas-solid flow, *J. Nat. Gas Sci. Eng.* 40 (2017) 91–113.
- [12] A.E. Carlos Varas, E. Peters, J.A.M. Kuipers, Computational fluid dynamics–discrete element method (CFD-DEM) study of mass-transfer mechanisms in riser flow, *Ind. Eng. Chem. Res.* 56 (19) (2017) 5558–5572.
- [13] K. Elsayed, C. Lacor, The effect of the dust outlet geometry on the performance and hydrodynamics of gas cyclones, *Comput. Fluids* 68 (2012) 134–147.
- [14] C. Liu, Z. Chen, W. Zhang, C. Yang, Y.a. Mao, Y. Yu, Q. Xie, B. Shotorban, Effects of Blade Parameters on the Flow Field and Classification Performance of the Vertical Roller Mill via Numerical Investigations, *Math. Probl. Eng.* 2020 (2020) 1–15.
- [15] M. Vatani, S.E. Ghasemi, D.D. Ganji, Investigation of micropolar fluid flow between a porous disk and a nonporous disk using efficient computational technique, *Proceedings of the Institution of Mechanical Engineers, Part E: Journal of Process Mechanical Engineering* 230 (6) (2016) 413–424.
- [16] H.A. Petit, C.I. Paulo, O.A. Cabrera, E.F. Irassar, Modelling and optimization of an inclined plane classifier using CFD-DPM and the Taguchi method, *App. Math. Model.* 77 (2020) 617–634.
- [17] A.D. Gosman, E. Ioannides, Aspects of computer simulation of liquid-fuelled combustors, *Energy* 7 (6) (1983) 482–490.
- [18] J. Gu, Y. Shao, X. Liu, W. Zhong, A. Yu, Modelling of particle flow in a dual circulation fluidized bed by a Eulerian-Lagrangian approach, *Chem. Eng. Sci.* 192 (2018) 619–633.
- [19] Y. Shao, J. Gu, W. Zhong, A. Yu, Determination of minimum fluidization velocity in fluidized bed at elevated pressures and temperatures using CFD simulations, *Powder Technol.* 350 (2019) 81–90.
- [20] P. Skjetne, J.E. Olsen, A parcel based modelling concept for studying subsea gas release and the effect of gas dissolution, *Progress in Computational Fluid Dynamics, An. Int. J.* 12 (2/3) (2012) 187.
- [21] A. Macías-García, E.M. Cuerda-Correa, M.A. Díaz-Díez, Application of the Rosin-Rammler and Gates-Gaudin-Schuhmann models to the particle size distribution analysis of agglomerated cork, *Mater. Charact.* 52 (2) (2004) 159–164.
- [22] Y.e. Qiu, H. He, C. Xu, B. San, Aerodynamic optimization design of single-layer spherical domes using kriging surrogate model, *Adv. Struct. Eng.* 24 (10) (2021) 2105–2118.
- [23] M. Cavazzuti, *Optimization Methods: From Theory to Design Scientific and Technological Aspects in Mechanics*, Springer, Berlin, 2013.
- [24] Y. Ji, Z. Yang, J. Ran, H. Li, Multi-objective parameter optimization of turbine impeller based on RBF neural network and NSGA-II genetic algorithm, *Energy Rep.* 7 (2021) 584–593.
- [25] D.R. Jones, M. Schonlau, W.J. Welch, Efficient Global Optimization of Expensive Black-Box Functions, *J. Glob. Optim.* 13 (4) (1998).